Ceramide lowering rescues respiratory defects in a *Drosophila* model of acid sphingomyelinase deficiency

Alexander J. Hull [ID][1], Magda L. Atilano [ID][1], Jenny Hallqvist[2], Wendy Heywood [ID][2], Kerri J. Kinghorn [ID][1,*]

[1]Institute of Healthy Ageing, Department of Genetics, Evolution and Environment, University College London, Darwin Building, Gower Street, London, WC1E 6BT, United Kingdom
[2]Great Ormond Street Institute of Child Health, University College London, 30 Guildford Street, London, WC1N 1EN, United Kingdom

*Corresponding author. Institute of Healthy Ageing, Department of Genetics, Evolution and Environment, University College London, Darwin Building, Gower Street, London, WC1E 6BT, United Kingdom. E-mail: k.kinghorn@ucl.ac.uk

Abstract

Types A and B Niemann-Pick disease (NPD) are inherited multisystem lysosomal storage disorders due to mutations in the *SMPD1* gene. Respiratory dysfunction is a key hallmark of NPD, yet the mechanism for this is underexplored. *SMPD1* encodes acid sphingomyelinase (ASM), which hydrolyses sphingomyelin to ceramide and phosphocholine. Here, we present a *Drosophila* model of ASM loss-of-function, lacking the fly orthologue of *SMPD1*, *dASM*, modelling several aspects of the respiratory pathology of NPD. *dASM* is expressed in the late-embryonic fly respiratory network, the trachea, and is secreted into the tracheal lumen. Loss of *dASM* results in embryonic lethality, and the tracheal lumen fails to fill normally with gas prior to eclosion. We demonstrate that the endocytic clearance of luminal constituents prior to gas-filling is defective in *dASM* mutants, and is coincident with autophagic, but not lysosomal defects, in late stage embryonic trachea. Finally, we show that although bulk sphingolipids are unchanged, dietary loss of lipids in combination with genetic and pharmacological block of ceramide synthesis rescues the airway gas-filling defects. We highlight myriocin as a potential therapeutic drug for the treatment of the developmental respiratory defects associated with ASM deficiency, and present a new NPD model amenable to genetic and pharmacological screens.

Keywords: lysosomal storage disorder; Niemann-Pick; sphingolipid; *Drosophila*; lysosome; *SMPD1*; *dASM*

Introduction

Types A and B Niemann-Picks disease (NPD) are multisystemic inherited disorders of metabolism caused by bi-allelic mutations in the *SMPD1* gene, of which more than 225 pathogenic variants have been identified [1, 2]. *SMPD1* encodes the lysosomal hydrolase acid sphingomyelinase (ASM), which cleaves the sphingolipid sphingomyelin (SM) into ceramide (Cer) and phosphocholine. In Types A and B NPD, SM accumulates in the lysosomes of engorged macrophages, termed foam cells, which infiltrate various tissues, including the liver, lungs, spleen and bone marrow to cause multiorgan disease. In Type A NPD, there is also primary neurological involvement [3]. Moreover, heterozygous *SMPD1* mutations were recently discovered to be a Parkinson's disease (PD) risk factor, although the exact mechanisms linking the two conditions are yet to be fully elucidated [4–6]. As well as this emerging genetic link, SM is found enriched in intracytoplasmic neuronal inclusions of aggregated *α*-synuclein protein, known as Lewy bodies, the main neuropathological hallmark of PD [7, 8].

ASM functions at low pH principally within the lysosome, hydrolysing SM in a zinc-independent manner as part of the lipid salvage pathway. It is also trafficked through the secretory pathway to act extracellularly on SM at the plasma membrane

in a zinc-dependent manner [9]. As expansion of the lysosomal compartment is the hallmark Niemann-Pick pathology, it is thought lysosomal ASM is the principal driver of the disease, yet the contribution of secreted ASM to Niemann-Pick or PD pathology has yet to be effectively resolved [10]. Several studies have demonstrated altered plasma membrane composition in *SMPD1* mutants, indicating that the function of ASM at the plasma membrane may be important to NPD pathology [11, 12].

Enzyme replacement therapy (ERT) with olipudase alfa was recently FDA improved for Types A and B NPD and is associated with a significant increase in lung diffusion capacity, and a reduction in both liver and spleen size [13–15]. However, ERT is costly and does not penetrate the blood brain barrier sufficiently to treat neurological disease. Thus, alternative therapies aimed at reversing ASM deficiency are greatly required. Here we present a *Drosophila* model of ASM loss-of-function, mutated in the fly orthologue of *SMPD1*, *dASM*. We show that loss of dASM function leads to embryonic lethality and developmental defects in the *Drosophila* respiratory system, mimicking those in patients with Types A and B NPD. We further demonstrate that these defects can be rescued by dietary, genetic and pharmacological manipulations that decrease lipid and sphingolipid abundance.

Results

Drosophila ASM is required for early development and is strongly expressed in the airway luminal cells

We first sought to develop a Types A and B NPD model in *Drosophila*, identifying *CG3376* as the closest *Drosophila* ortholog of human *SMPD1* (Fig. 1A) (Supplementary Fig. 1). A NCBI conserved domain search identified a conserved saposin-like domain and a conserved ASMase domain with 73% sequence homology across the domain (Fig. 1B). We henceforth refer to *CG3376* as *dASM*.

A range of *dASM* mutants were available, including an un-excised p-element in the 5′ (*dASM^k^*), a CRISPR-derived frameshift indel in the 5′ coding region (*dASM^22.7.2^*), a full excision of the gene (*dASM^KO^*) and a truncation mutant caused by insertion of a Gal4-containing transgenic element into the 3rd intron (*dASM^CRIMIC^*) (Fig. 1A). We identified a significant lifespan shortening effect in *dASM^KO^* heterozygotes (Fig. 1C), suggesting a requirement in adulthood for *ASM* in *Drosophila,* as well as during development. All mutants tested were homozygous lethal.

Balancing *dASM* mutants over CyO-GFP allowed us to track homozygous flies throughout early development and to identify lethal timepoints from which we could infer a requirement for dASM activity. At late stage 17, the developmental stage immediately prior to hatching, we identified morphologically normal *dASM^−/−^* embryos exhibiting sequential muscle contractions. However, no viable 1st instar larvae of any *dASM* homozygous mutant strain emerged post-hatching (Fig. 1D), indicating that complete loss of dASM activity is lethal at late embryonic stages. As all tested *dASM* mutants phenocopy one another, we ascertained that they are all loss-of-function lines and elected to do most of the subsequent experiments with the *dASM^k^* mutant.

To identify the tissues requiring dASM function, we tested the expression pattern of *dASM* in late embryonic development by crossing the *dASM^CRIMIC^* line, which contains a Gal4 insertion in the coding region [16], to a nuclear localised mCherry (UAS-mCherry.nls). We identified strong ubiquitous staining in both the epidermis and the tracheal luminal cells at stage 17 (Fig. 1E). This tracheal expression is corroborated by *in-situ* hybridisations from the Berkeley *Drosophila* Genome Project (BDGP) that reveal that the *dASM* transcript in late-stage embryos is enriched in expression in the trachea [17].

We then studied expression patterns of a GFP-tagged *dASM* construct expressed under an endogenous promoter from the fTRG library [18]. At stage 16, prior to tracheal gas-filling, we identified GFP aggregates in vacuole-like structures within the tracheal lumen, suggesting dASM is secreted into this cavity. We also observed GFP staining within vesicles of the tracheal cells following gas-filling at stage 17, indicating the presence of dASM within the endolysosomal network (Fig. 1F).

dASM activity is required for tracheal gas-filling

At stage 17, in the hours prior to eclosion, the embryonic trachea in *Drosophila* are morphologically mature, but undergo a transition whereby the liquid layer of the lumen is replaced with a functional gas layer in a sequential cell-specific manner, to allow oxygen exchange and physiological functions [19]. Given the strong expression pattern of dASM within the trachea, we assessed *dASM^k^* mutants under the light microscope to determine if any structural changes in the tracheal system, preceding the embryonic lethality, were apparent. This demonstrated that there were severe gas-filling defects in all embryonic lethal *dASM* mutants (Fig. 2A).

To validate the fact that this defect was related to tracheal expression of dASM, we expressed RNAi against *dASM* under the control of the tracheal-specific driver Btl-GAL4. This resulted in a mild but statistically significant decrease in gas-filling, confirming that the loss of tracheal dASM drives the gas-filling defect (Fig. 2B).

To establish whether this gas-filling abnormality was dependent on loss of ASMase domain activity, we tested a mutant possessing a CRISPR-generated point mutation (R571L) in the active site of the ASMase domain of *Drosophila dASM* (Fig. 1A), corresponding to the R496L point mutation in human *SMPD1*. This common missense mutation results in a near-complete loss of ASMase activity and is associated with Type A NPD [20, 21]. *dASM^R571L^* homozygotes showed a robust loss of tracheal gas-filling (Fig. 2C). To further validate that loss of the ASMase domain function is causative for the air-filling defects, we injected desipramine, a potent ASMase inhibitor into control blastoderm-stage embryos. This resulted in a statistically significant dose-dependent reduction in tracheal gas-filling at late-stage 17 (Fig. 2D). Staining with DHE, a marker of superoxide species production, suggested significantly higher reactive oxygen species (ROS) levels in the trachea of *dASM^k^* mutants compared to controls, potentially a consequence of tissue hypoxia, or an indication of redox defects that may regulate gas-filling (Fig. 2E).

Tracheal endocytosis and luminal clearance are disrupted in *dASM* mutant embryos

To assess if loss of *dASM* causes gross structural tracheal defects, we probed tracheal morphology at stage 15 by staining with an antibody against Gasp. This is a secreted chitin-binding protein present in the tracheal lumen, and thus immunostaining for this intrinsic component allows visualisation of the entire tracheal network. Patterns of tracheal branching in stage 15 embryos appeared unchanged between control and *dASM^k^* mutant flies, with a full complement of primary and secondary tracheal branches, including morphologically normal dorsal and lateral trunks and dorsal, visceral and ganglionic branches (Fig. 3A). Previously characterised tracheal defects such as tube over-elongation, or defects in tube fusion were not observed, excluding the possibility that these defects in early morphogenesis underlie the gas-filling abnormalities [22].

Tracheal luminal development has been extensively characterised in a temporal fashion. Exocytic events from tracheal luminal cells stimulate development of a chitin exoskeleton, which regulates diameter expansion. As morphogenetic changes are completed, this exoskeleton is degraded by a pool of secreted chitinases. The resulting milieu of luminal constituents is then resorbed by the tracheal epithelia through endocytosis, presumably resulting in degradation via the endolysosomal network [23].

Immunostaining *dASM^k^* embryos for Gasp at stage 16, when chitin levels are reduced, revealed a significant increase in staining within the tracheal lumen of *dASM^k^* mutants, indicative of impaired chitin clearance (Fig. 3B). We next expressed a fluorescently tagged chitin-binding protein Cht-TOM under the tracheal driver in *dASM^k^* mutants. In control flies, dispersed chitin staining was visible throughout the tracheal lumen at stage 15 and transitioned to the luminal border by late stage 17, as previously described [23]. In *dASM^k^* mutants, however, Cht-TOM remained luminal into late stage 17 as evidenced by increased fluorescence intensity within the tracheal lumen, indicative of decreased chitin clearance (Fig. 3C). We next expressed the chitin-modifying protein, Verm-RFP, which in controls showed a shift throughout development from a primarily luminal location at stage 15,
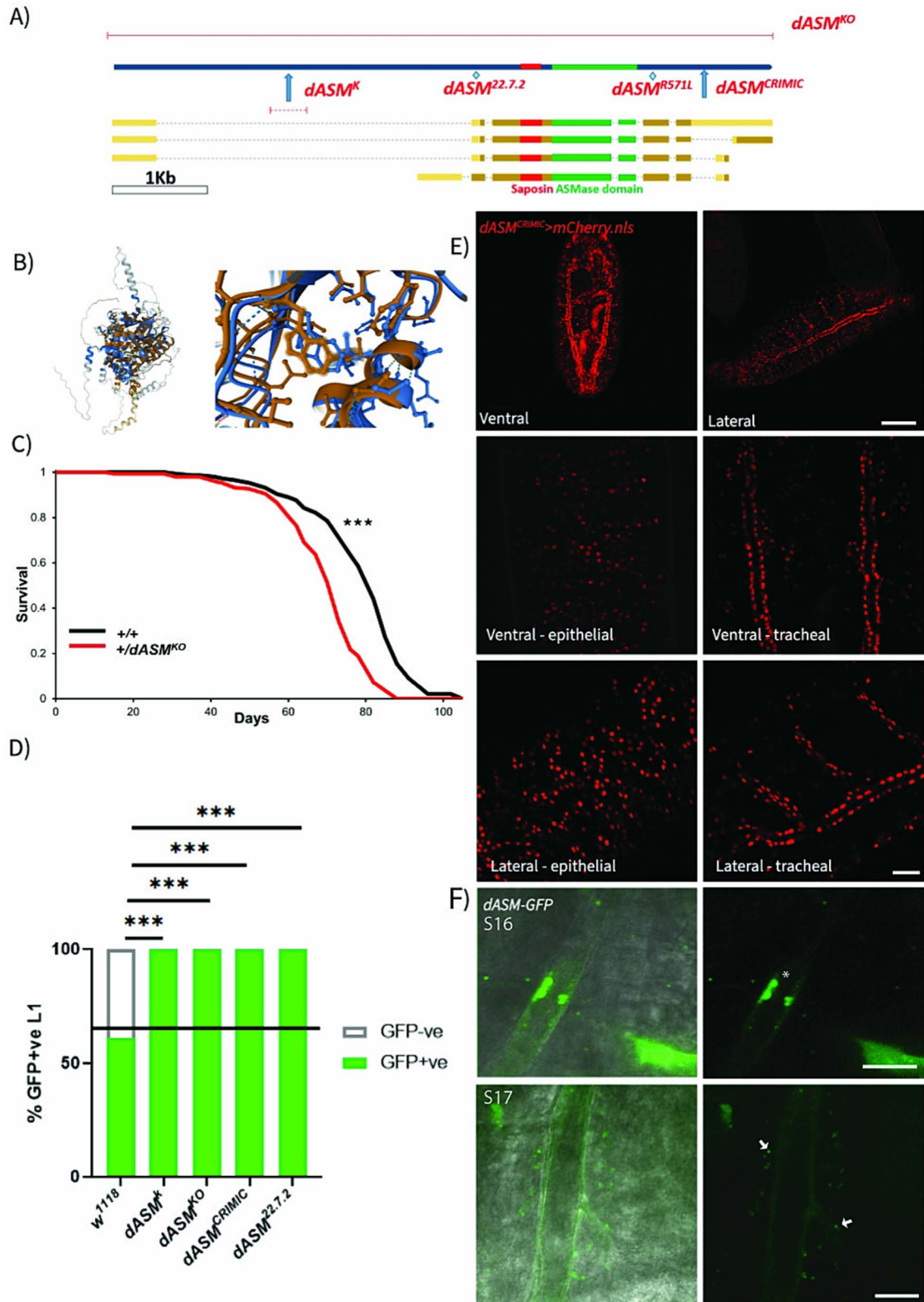
Figure 1. *Drosophila* dASM is required for developmental viability. (A) Annotated schematic of the *CG3376/dASM* coding region and the sites of available mutants. (B) Alphafold prediction of human ASM (blue) and *Drosophila* dASM (orange) secondary structures, full view (left), and a close-up of the ASMase active site (right). (C) Survival curves of *dASM*^{KO} heterozygote and control flies (n = 150, log rank tests, $P < 0.0001$). (D) Schematic of crossing scheme and quantification of GFP +ve heterozygous to GFP −ve homozygous 1st instar larvae (n = 272, 293, 151, 403, 113. w^{1118} vs *dASM*$^{k/KO/CRIMIC/22.7.2}$, $P < 0.0001$***, χ^2 test). (E) Dorsal and ventral views of the localisation of dASM expression in the trachea and epidermis of stage 17 embryos using *dASM*^{CRIMIC} > *mCherry.nls*. Scale bar = 100 μm for whole embryos, and 25 μm for 63× magnification images. (F) Localisation of dASM-GFP within the tracheal lumen at stage 16 (asterisk) and in vesicles within the tracheal epithelia (arrows) and on the luminal edge at stage 17, scale bar = 10 μm.
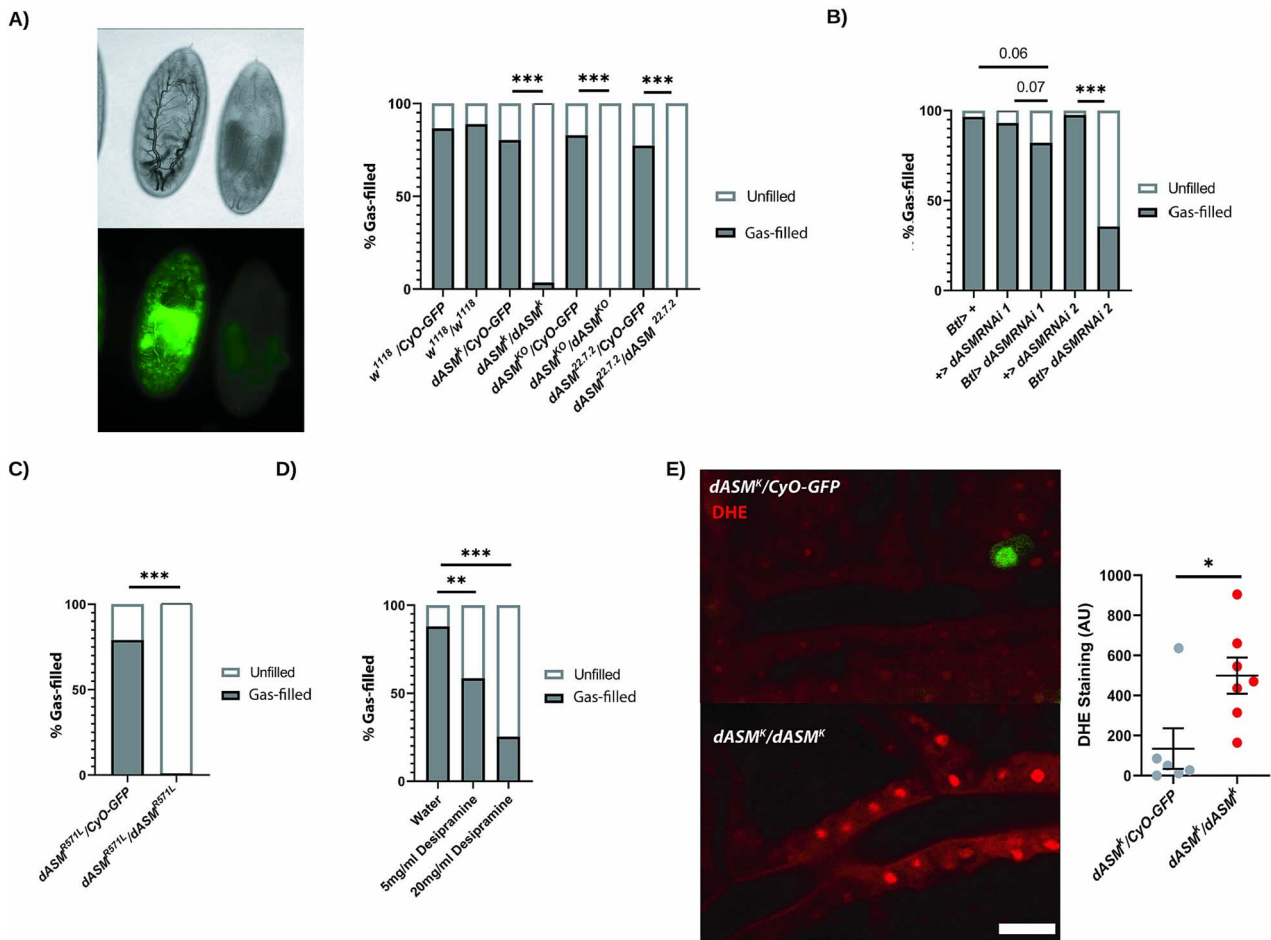
Figure 2. dASM mutants display tracheal gas-filling defects. (A). Example brightfield image of stage 17 heterozygous (GFP +ve) and homozygous (GFP −ve) *dASM^k* embryos, demonstrating a loss of tracheal gas-filling. Quantification of airway gas-filling in *dASM* mutants and controls (n = 18, 52, 57, 173, 101, 204, 31, 44, w^{1118} vs $dASM^{k/KO/CRIMIC/22.7.2}$, P < 0.0001, χ^2 test). (B) Quantification of gas-filling defects following tracheal specific expression (Btl-GAL4) of RNAi against *dASM* (n = 29, 58, 56, 78, 76, *dASM* RNAi 1 vs Btl > *dASM* RNAi 1 P = 0.07, *dASM* RNAi 2 vs Btl > *dASM* RNAi 2 P < 0.0001, χ^2 test). (C) Gas-filling defects in $dASM^{R571L}$ embryos containing a point mutation in the ASMase domain (n = 220, 95, P < 0.0001, χ^2 test). (D) Quantification of gas-filling defects in stage 17 embryos injected with either desipramine (des) or water 30 min after egg-laying (n = 50, 41, 67, PBS vs 5 mg/ml des P = 0.0013, PBS vs 20 mg/ml des P < 0.0001, χ^2 test). (E) Example image and quantification of DHE staining in late stage 17 *dASM^k* mutant and control (*dASM^k*/CyO-GFP) tracheal lumens showing a significant increase in ROS (P = 0.0207, t-test), scale bar = 10 μm.

localising to intracellular vesicles of the tracheal epithelial cells by late stage 17. In *dASM^k* mutants, significantly higher expression of Verm-RFP was retained in the lumen compared to controls (Fig. 3D). Taken together, these data demonstrate that chitin removal, but not deposition, is disrupted in *dASM^k* mutants.

It has previously been established that the clearance of luminal contents, principally degraded chitin and its associated modifiers, is contingent on an endocytic burst [23]. To investigate this, we expressed the secreted factor ANF::GFP in tracheal cells. In controls, ANF::GFP was secreted into the lumen and visible at stage 15, and subsequently cleared by late stage 17, demonstrating both functional exocytic secretion and endocytic uptake. In *dASM* mutants, by contrast, ANF::GFP was deposited in the lumen at stage 15, and not within visible intracellular aggregates, showing that exocytosis is functional. However, by late stage 17, statistically significant elevation in ANF::GFP fluorescence was observed in the tracheal lumens of *dASM* mutants, demonstrating a failure to specifically endocytose luminal constituents (Fig. 3E). In late stage 17 *dASM^k* mutants, but not in controls, spherical vacuolated structures were also visible in the tracheal lumen that excluded ANF, Cht or Verm markers. It is unknown if these

structures are membranous or if they originate as secreted vesicles.

To study the ultrastructure of *dASM^k* tracheal lumens in greater detail, we next performed transmission electron microscopy (TEM) on transverse sections of stage 17 *dASM^k* mutant and control embryos. In keeping with our fluorescent imaging data, we observed incomplete chitin remodelling at the luminal periphery and a failure to produce distinct taenidial folds at the tracheal luminal edge (Fig. 3F). In addition to the vacuolated structures seen within the tracheal lumen on fluorescent imaging, there was also evidence of luminal debris. From this data, we can conclude that *dASM* is required for tracheal development in late embryogenesis, specifically for the clearance of luminal constituents prior to gas-filling.

To further determine the nature of this remodelling defect, given the finding from ANF::GFP expression that there is impairment of tracheal cell endocytosis, we expressed a range of vesicular markers related to the endo-lysosomal system under the control of a tracheal driver. Deeper into the endosomal network, expression of the autophagosome marker mcherry-Atg8 revealed a significant decrease in the size and intensity of autophagosomes
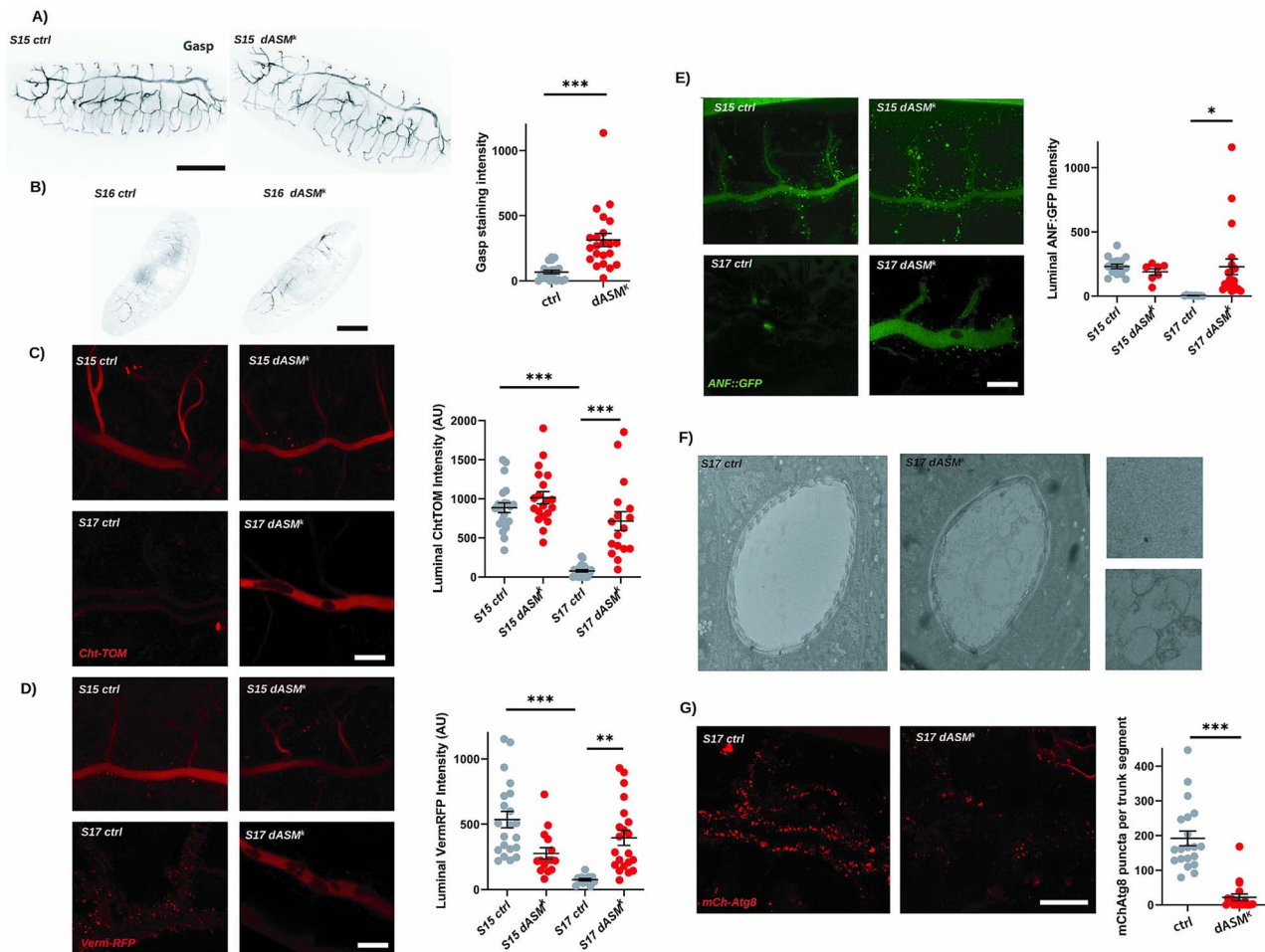
Figure 3. *dASM* mutants exhibit defects in the clearance of chitin from the tracheal lumen during development. (A) Images of whole tracheal morphology of stage 15 control (ctrl) and *dASM^k* flies stained for Gasp, highlighting that all elements of the tracheal network are intact, scale bar = 100 μm. (B) Example confocal images of early stage 16 ctrl or *dASM^k* embryos stained for Gasp and quantification of luminal staining intensity (P = 0.0003, t-test), scale bar = 100 μm. (C) Example confocal images of ctrl and *dASM^k* embryos at stage 15 and 17 expressing Btl > ChtTOM and quantification of staining intensity across the tracheal lumen (S15 ctrl vs S17 ctrl P < 0.0001, S17 ctrl vs S17 *dASM^k* P < 0.0001, one-way ANOVA with Tukey's multiple comparisons test), scale bar = 25 μm. (D) Example confocal images of ctrl and *dASM^k* embryos at stage 15 and late stage 17 expressing Btl > VermRFP and quantification of staining intensity across the tracheal lumen (S15 ctrl vs S17 ctrl P < 0.0001, S17 ctrl vs S17 *dASM^k* P = 0.0015, one-way ANOVA with Tukey's multiple comparisons test), scale bar = 25 μm. (E) Example confocal images of ctrl and *dASM^k* embryos at stage 15 and 17 expressing Btl > ANF::GFP and quantification of staining intensity across the tracheal lumen (S15 ctrl vs S17 ctrl P = 0.0233, S17 ctrl vs S17 *dASM^k* P = 0.0176, one-way ANOVA with Tukey's multiple comparisons test), scale bar = 25 μm. (F) Transverse TEM section of the dorsal trunk in ctrl and *dASM^k* stage 17 embryos. (G) Example confocal images of stage 17 ctrl and *dASM^k* embryos expressing Btl > mCh-Atg8 and quantification of staining intensity (P < 0.0001, t-test), scale bar = 25 μm.

in *dASM^k* mutant tracheal cells (Fig. 3G). These findings suggest that a disruption of the broader vesicular network may underlie defects in luminal clearance.

dASM loss-of-function is associated with changes in Cer saturation in the absence of abnormalities in lysosomal morphology in late embryonic trachea

As NPD is a lysosomal storage disorder, characterised by lysosomal dysfunction and expansion of the lysosomal compartment [24], and because we identified defects at other points in the vesicular network, we stained stage 17 *dASM^k* embryos with Lysotracker, a dye specific to acidified vesicles. Curiously, no significant difference in the abundance of lysosomal puncta was observed in the *dASM* mutant tracheal luminal cells compared with controls (Fig. 4A). This suggests that tracheal defects in *dASM* mutant embryos do not stem from late-stage lysosomal dysfunction, but rather a mechanism of action beyond the lysosome. As

dASM-GFP appears to be punctate and secreted into the tracheal lumen (Fig. 1F), it is likely dASM may be secreted and function at the extracellular surface of the plasma membrane. Furthermore, we observed no changes in Lysotracker staining in the epidermis, or in mosaic *dASM^k* mutants in 3-week-old gut or fat bodies (Supplementary Fig. 2), suggesting lysosomal defects do not occur in other tissues.

To assess if there was macrophage involvement in the respiratory pathology, as is the case in NPD, we visualised hemocytes with the cytoskeletal marker srpHemo-Moe.mCherry. This failed to demonstrate any instance of macrophages contacting or infiltrating the tracheal network in either control or *dASM* mutants (Fig. 4B).

Furthermore, there were no changes in the levels of the lysosomal marker LAMP1 in whole late stage 17 embryos (Fig. 4C), supporting the fact that bulk lysosomal defects are not present in the tracheal tissue of *dASM* deficient mutants at this developmental timepoint. Similarly, there was no significant difference in staining for active Caspase 3, a marker of apoptosis, excluding
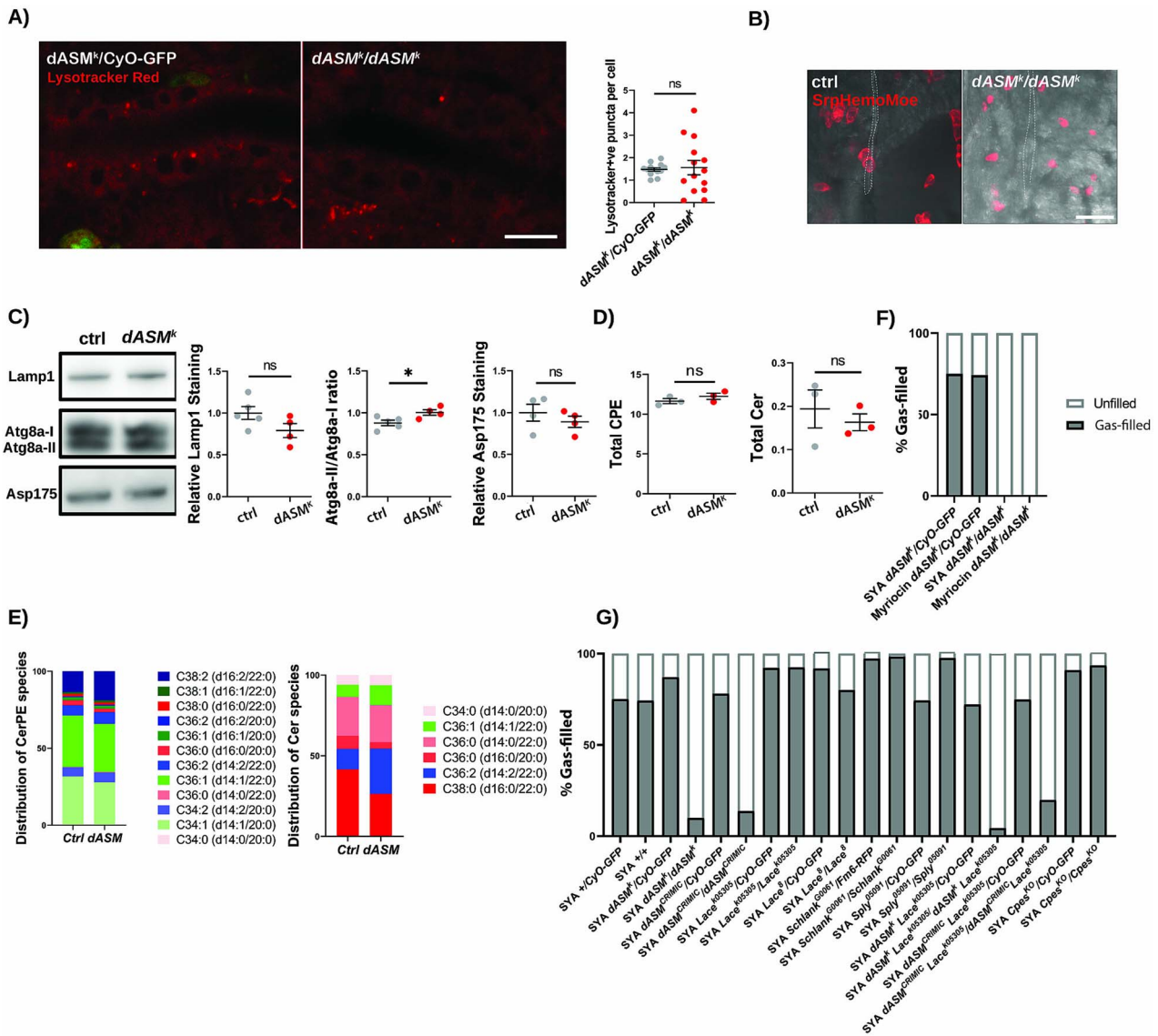
Figure 4. *dASM* mutants fail to demonstrate macrophage ingression, lysosomal expansion or changes in bulk sphingolipid abundance. (A) Example images showing Lysotracker red DND99 staining within stage 17 ctrl and *dASM^k* tracheal cells and quantification (P = 0.8113, t-test), scale bar = 10 μm. (B) Representative images of macrophages (Srp.Hemo.Moe.mCherry) and trachea (Brightfield) showing no colocalisation or infiltration of macrophages in ctrl or *dASM^k* mutants, scale bar = 25 μm. (C) Western blots on whole stage 17 ctrl or *dASM^k* embryo extracts. Example images and quantification normalised to actin for Lamp1 (P = 0.1094. t-test), Atg8a-II/I ratio (P = 0.003, t-test) and Asp175 (P = 0.4025, t-test), demonstrating no change in embryo-wide lysosomal or apoptotic activity. (D) Graphs of overall abundance of ceramide (Cer) and Cer phosphoethanolamine (CPE) in ctrl or *dASM^k* mutant stage 17 embryos (ctrl vs *dASM^k* CPE P = 0.2943, ctrl vs *dASM^k* Cer P = 0.5532, t-test) as detected by HPLC. (E) Graph of sphingolipid species by chain length and saturation state in ctrl or *dASM^k* mutant stage 17 embryos. (F) Quantification of gas-filling defects in *dASM* flies with myriocin or DMSO supplementation in the maternal diet. (G) Quantification of gas-filling in mutants of sphingolipid biosynthesis alone or in combination with the *dASM^k* mutant, all raised on a standard diet of sugar-yeast-agar (SYA).

widespread cell death in *dASM^k* mutants (Fig. 4C). A significant increase was detected in both Atg8a-II and the Atg8a-II/Atg8a-I ratio, indicative of increased autophagosome formation, likely related to hypoxic tissue degradation (Fig. 4C).

We next assessed the abundance of Cer phosphoethanolamine (CPE), the fly analogue of SM, and its putative derivative Cer using HPLC [25]. The overall abundance of CPE or Cer was not altered in *dASM* embryos compared to controls (Fig. 4D). Similarly, no significant differences in chain length or saturation were evident among the classes of CPE, demonstrating that CPE is unchanged in *dASM* deficiency. Significant changes were, however, identifiable within the Cer species, with an increase in unsaturated ceramides in

dASM^k mutants (Fig. 4E). The mechanism of this shift and its functional relevance is unknown; however, unsaturated sphingolipids possess decreased density and interaction with cholesterol within a membrane. Thus, changes in Cer saturation may affect lipid raft stability within membranes with consequent effects on vesicle dynamics [26, 27].

Together, this data suggests that the nature of the respiratory defects observed in *dASM* mutants depart from canonical NPD pathology, with no obvious progressive change in lysosomal area or sphingolipid abundance. It is feasible that minor effects of *dASM* deficiency in the trachea are not detectable in a whole fly homogenate. However, more likely is the possibility that *dASM* is

secreted, as has been proposed elsewhere [28], acting on CPE at the membrane to facilitate signalling events at a level imperceptible to bulk biochemical analysis.

Cer is a central sphingolipid at the centre of sphingolipid metabolism and is known to promote cell cycle arrest and cellular senescence [29]. Indeed, its intracellular abundance has been linked to many diseases, including neurodegenerative disorders such as PD and metabolic conditions, such as diabetes mellitus [30–33]. To determine if the gas-filling defects are influenced by Cer abundance, we raised maternal flies on media containing myriocin, a potent serine-palmitoyl transferase (SPT) inhibitor that blocks de-novo Cer synthesis [34]. This manipulation had no effect on the gas-filling defects of *dASM^k* embryos (Fig. 4F).

To directly measure the impact of zygotic sphingolipid synthesis on gas-filling, we screened and found no gas-filling defects in control embryos mutant for *Lace (SPT)*, *Schlank* (Cer synthase), *Sply* (sphingosine phosphate-1-lyase) and *CPES* (CPE synthase) (Fig. 4G). Knockdown of SPT using the *Lace^k05305* mutant in *dASM^k* mutants, resulting in a condition of presumptively lower Cer, did not alter the gas-filling defects (Fig. 4G).

The gas-filling defects observed in dASM deficient flies are rescued by a combination of restricting dietary lipids and zygotic Cer biosynthesis

Our data suggest that dASM is required in an extra-lysosomal manner for clearance of tracheal proteins, and as an ostensible lipid hydrolase. We therefore hypothesised that dASM might modify lipid constitution at the membrane. We thus reasoned that modulating the abundance of certain lipids in the plasma membrane might influence the *dASM* mutant gas-filling defect.

We aimed first to disrupt bulk lipid bioavailability and then specifically sphingolipid metabolism (Fig. 5A). As maternal synthesis, zygotic synthesis and dietary presence of lipids could all influence lipid availability, we began a combinatorial approach to shift membrane lipid constitution. We made the following assumptions about lipid homeostasis in the late embryo: A) zygotic lipid constitution will be influenced by the maternal deposition of lipids; and B) egg production occurs in adulthood, so the deposition of lipids in the ovaries will be influenced by the adult maternal diet and lipid synthesis. We therefore raised *dASM^{k/+}* heterozygote mothers on a holidic pre-defined diet to selectively add and remove elements [35]. As *Drosophila* are sterol auxotrophs [36, 37], the only lipid in holidic medium is cholesterol, and all other lipids in the embryo must be synthesised de-novo by maternal or zygotic synthesis pathways. To our surprise, raising maternal *dASM^k* heterozygote flies on a holidic medium for 6 days, and during mating, was sufficient to uncover a robust population of *dASM^k* homozygote mutant progeny with gas-filled trachea (Fig. 5B).

As sterols are a key constituent of lipid rafts and may form microdomains with sphingolipids in membranes [38], we removed or over-supplemented cholesterol in a holidic diet at 0×, 1× and 6× cholesterol. None of these supplemented cholesterol concentrations led to an alteration in gas filling defects in *dASM^k* mutants (Fig. 5C). To determine if the gas-filling rescue was related to lipid bioavailability, we supplemented holidic medium with 20% sugar, which is a substrate for lipid synthesis following glycolysis and fatty acid synthesis, and found sugar significantly abrogated gas-filling in *dASM^k* mutants on holidic media (Fig. 5D) [39]. Direct supplementation of holidic medium with 3% coconut oil or lard resulted in a complete cessation of egg-laying. Therefore, we

conclude from these findings that maternal dietary lipids are required for the maintenance of lipid membranes and that dASM is an essential regulator of membrane remodelling and homeostasis.

To assess if gas-filling defects were related to the overabundance of Cer species, we inhibited zygotic Cer synthesis using a *Lace^k05305*; *dASM^k* double mutant. Whilst loss-of-function *Lace* mutations alone had no deleterious effect on gas-filling, in combination with a holidic medium, *Lace^k05305*; *dASM^k* double mutants displayed a significantly higher airway gas-filling percentage than *dASM^k* mutants alone. These findings suggest that lowering Cer reduces the tracheal defects in *dASM* mutant embryos (Fig. 5E). To further test this hypothesis, we incorporated myriocin, an inhibitor of SPT in the Cer synthesis pathway, into the maternal holidic diet. Supplementation with myriocin significantly increased the gas-filling rescue of the holidic diet in *dASM* mutants (Fig. 5F). Taken together, this data suggests that an overabundance of a Cer species, or a derivative, leads to a gas-filling tracheal defect, which requires dASM ASMase domain activity to overcome. Thus, Cer lowering offers a potential therapeutic strategy requiring further functional exploration in preclinical models or clinical trials in Types A and B NPD and associated disorders.

Discussion

Types A and B NPD are rare lysosomal storage disorders characterised by multi-organ involvement, with interstitial lung disease a well-recognised feature [3]. Olipudase alfa is a recently approved ERT and remains the most promising therapeutic strategy for non-neuronopathic manifestations of NPD [13, 14, 40]. However, its use is associated with high treatment costs, limiting its availability in some countries. There thus remains a need to further develop novel therapeutics to be used alone or in combination with ERT. Here we present a novel NPD model through loss of the fly *dASM*.

We demonstrated that *dASM* mutants display defects in respiratory luminal clearance. As macrophages do not infiltrate the trachea in *Drosophila,* and were not seen to do so in *dASM* mutants, it is likely that tracheal cells, known to be endocytically active, have an analogous function to macrophages in mammals in turning over luminal constituents [41]. The absence of lysosomal or macrophage phenotypes in tracheal cells raises the possibility that respiratory defects in humans may not arise solely from canonical lysosomal storage defects, but rather secondary to other pathologies, perhaps related to the secretory functions of ASM.

dASM mutant embryos lack several of the key hallmarks of NPD at the point of lethality in late-stage embryogenesis, namely lysosomal dysfunction and sphingolipid accumulation. Our data implies that loss of dASM leads to developmental extracellular defects in the tracheal lumen and targeted effects on membrane dynamics. It supports a possible secreted, rather than lysosomal role, in the developmental respiratory phenotypes of dASM deficiency. Consistent with our results, it was recently shown that dASM is primarily localized to the lysosome and is also secreted into the extracellular space [28]. Thus, this model has the potential to uncover previously understudied mechanisms of disease pathogenesis. Moreover, evidence of an increase in autophagosomes in the tracheal luminal cells is in keeping with other *Drosophila* LSD models, suggesting common mechanisms between diverse LSDs [42–44]. Furthermore, *dASM* is abundantly expressed in adulthood in the glia and fat body, indicative of
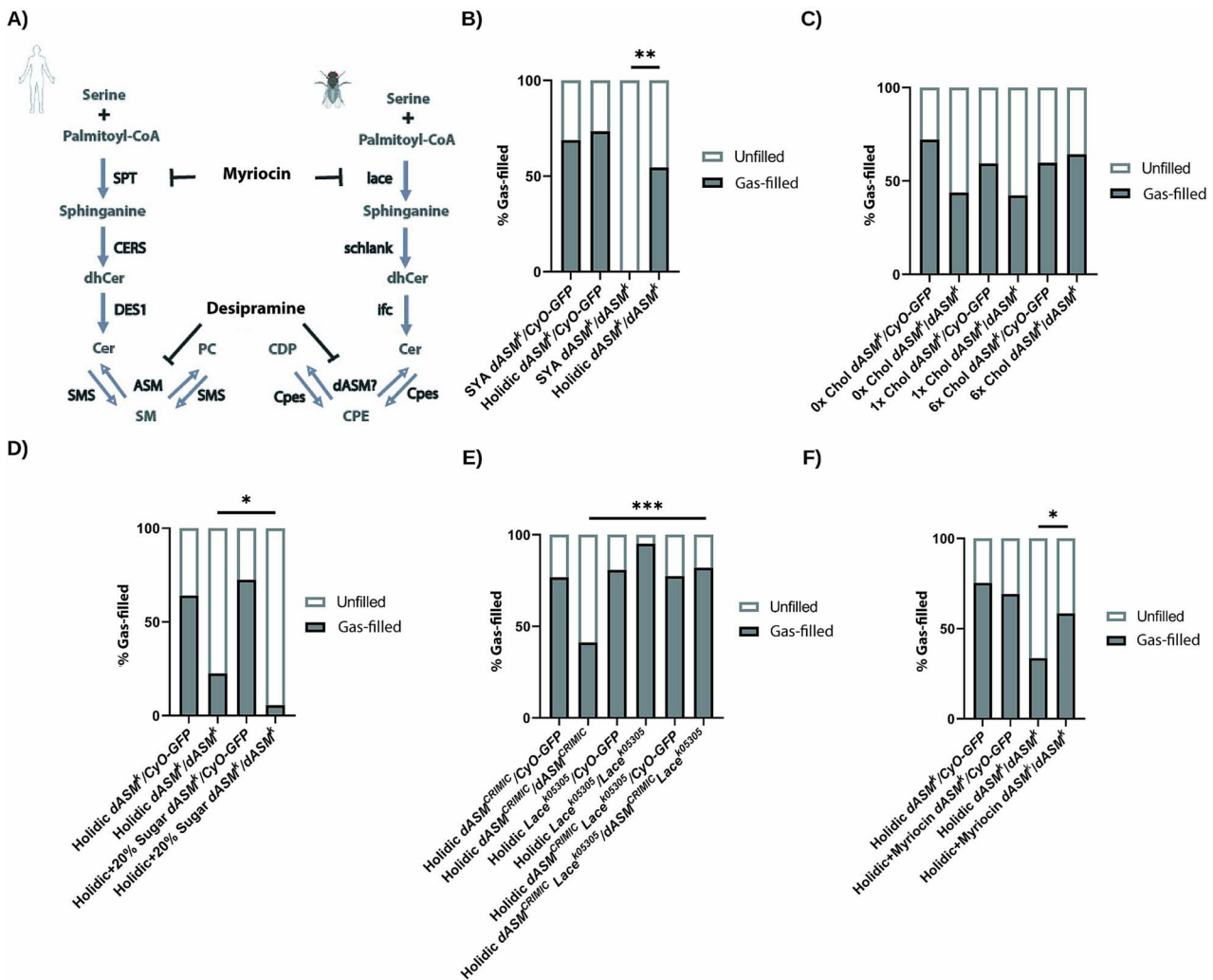
Figure 5. Dietary lipid restriction alongside genetic and pharmacological restriction of Cer synthesis alleviates *dASM* tracheal gas-filling defects. (A) Diagram of sphingolipid synthesis pathways in mammals and *Drosophila*. (B) Quantification of gas-filling defects in ctrl or *dASM*^{k} stage 17 embryos from maternal flies raised on SYA medium or a holidic diet (n = 45, 83, 16, 33, SYA *dASM*^{k} vs holidic *dASM*^{k} $P = 0.0002$, χ^2 test). (C) Quantification of gas-filling defects in ctrl or *dASM*^{k} stage 17 embryos from maternal flies raised on a holidic diet with 0×, 1× or 6× dietary cholesterol, showing no significant effect of cholesterol supplementation (n = 43, 64, 67, 16, 26, 28, 0× Chol *dASM*^{k} vs 1× Chol *dASM*^{k} $P = 0.9269$, 1× Chol *dASM*^{k} vs 6× Chol *dASM*^{k} $P = 0.1056$, χ^2 test). (D) Quantification of gas-filling defects in ctrl or *dASM*^{k} stage 17 embryos from maternal flies raised on a holidic diet with 0 or 20% sugar (n = 106, 53, 91, 36, $P = 0.0298$, χ^2 test). (E) Quantification of gas-filling defects in ctrl and *dASM*^{k} stage 17 embryos from maternal flies combining *Lace*^{K05305} raised on a holidic diet (n = 99, 34, 120, 41, 195, 78, *dASM*^{CRIMIC} vs *dASM*^{CRIMIC} *Lace*^{K05305} $P < 0.0001$, χ^2 test). (F) Quantification of gas-filling defects in ctrl or *dASM*^{k} stage 17 embryos from maternal flies raised on a holidic diet with or without myriocin supplementation (n = 199, 156, 86, 77, *dASM*^{k} ctrl vs *dASM*^{k} myriocin $P = 0.0016$, χ^2 test).

important roles in adulthood, and adult-specific knockout of *dASM* may produce more canonical LSD phenotypes.

Whilst pulmonary disorders are commonly reported across NPD types, their aetiology is understudied and inconclusive. One study found uniform pulmonary involvement manifesting either as COPD or chronic respiratory failure [45], and another showed 90% of Type A NPD patients died of respiratory failure [46]. In the milder form of the disease, Type B NPD, a high proportion of patients showed evidence of lung dysfunction [47]. Only individual case studies have specified respiratory pathology, with foam cells within the airway frequently identified [45], alongside interstitial lung disease [48], pulmonary alveolar proteinosis [49], and macrophage infiltration. An *Smpd1* knockout mouse model demonstrated a 'foam' phenotype macrophage accumulation within the airways, in addition to crystalline aggregation of chitinase-like-protein YM1 [50].

Our genetic and pharmacological data using a *Lace* mutant and myriocin strongly point towards abundance of Cer or a Cer derivative as being restrictive to airway gas-filling. It has previously been shown that CPE is an SM analogue in *Drosophila*, required for the formation of lipid rafts and their most abundant constituent [25]. Lipid rafts are key to major membrane-trafficking processes such as clathrin-independent endocytosis and exocytosis, and play diverse roles in anchoring and organising membrane proteins [30, 51]. ASM has been shown to induce spontaneous vesicle formation in artificial liposomes through the generation of ordered Cer domains [52]. Furthermore, exocytosed ASM is required for injury-dependent endocytosis at the plasma membrane, and accordingly, ASM-deficient cells are endocytosis-deficient [53]. We have shown ANF::GFP, a secretion marker, is not cleared from *dASM*^{k} tracheal lumens, suggesting a defect in endocytic uptake of luminal constituents. It is therefore possible

that dASM functions at the tracheal membrane in *Drosophila* in a similar manner to ASM in cell lines, to co-ordinate membrane budding events.

Our lipidomic analysis did not show elevated CPE, the putative substrate of dASM, at least not at the organismal level. It is, however, possible that there are tissue-specific changes in CPE within *dASM* mutants that we were unable to detect with our whole embryo analysis, or that dASM may target other sphingolipids. Though previous lipidomic analyses have failed to identify native SM in *Drosophila*, including in embryos, it is possible SM derived from the diet could be present and functional in understudied tissues [25, 54–56]. As point mutations in the active site of ASMase cause gas-filling defects, it is likely the enzyme functions through cleavage of a SM-like lipid. Intriguingly, the chitin subunit N-acetylglucosamine is a common lipid modification, and membrane-chitin meshworks may be involved in structuring chitin remodelling. dASM may therefore be developmentally required to cleave chitin-modified sphingolipids in the tracheal lumen.

Another lipid-modifying enzyme that has been implicated in tracheal gas-filling is *Wunen*, a secreted lipid phosphate phosphatase that principally dephosphorylates sphingolipids such as sphingosine-1-phosphate and Cer-1-phosphate. However, *Wunen* loss-of-function mutants have different tracheal phenotypes to *dASM* mutants, displaying defects in lumen fusion and accumulation of luminal proteins, indicative of the fact that they are not regulating the same pathway [57].

Whilst this manuscript was in preparation, a similar paper describing tracheal defects in *dASM* loss-of-function was published [28], focusing on the mechanisms of lysosomal dASM secretion into the lumen. They demonstrated that luminal lipids are derived from exocytosed MVB vesicles. In concordance, we also see vacuolated structures in the lumen of *dASM^k* mutants through TEM and fluorescent imaging. As defects in the number and location of various intracellular vesicles are present in *dASM^k* tracheal cells, we speculate broad defects in vesicle sorting occur in these cells, likely contingent on a dysregulation of membrane microdomains required for these events.

Crucially, the gas-filling phenotypes we identify are visible by light microscopy and require little preparation. Consequently, *dASM* mutants can be quickly screened for genetic, dietary or pharmacological modifiers, and have the potential as a tool to uncover novel therapies for Types A and B NPD. Using this model, we have demonstrated that reducing Cer levels via genetic or pharmacological means, when flies are reared under a maternal diet lacking Cer, leads to a reversal of the gas-filling tracheal defects. Thus, Cer lowering represents a potential therapeutic strategy for the respiratory pathology in Types A and B NPD and indeed, myriocin, an inhibitor of the Cer synthesis pathway, is already FDA-approved for use in humans. Thus, this work highlights the promise of re-purposed drugs like myriocin to be further studied in pre-clinical models, with the potential to be fast tracked into accelerated clinical trials in Types A and B NPD.

Materials and methods
Fly stocks and culture

Unless otherwise described, flies were raised on sugar-yeast-agar (SYA) medium and maintained at 25°C and 50% relative humidity on a 12:12 light–dark cycle. For embryo collections, except for dietary modifications, flies were placed onto grape juice agar plates. Following synchronisation, embryos were allowed to develop at 25°C (12 h for stage 16, 23 h for late stage 17).

Holidic medium was prepared as previously described [35]. For drug experiments, myriocin was dissolved in DMSO and added to the food to give a final concentration of 100 μM.

Flies were backcrossed over 6 generations into a w^{1118} background to reduce background effects. The following stocks were obtained from the Bloomington *Drosophila* Stock Centre (BDSC): *dASM^{CRIMIC}* (#91346), *dASM^{KO}* (#81092), *dASM^{R571L}* (#81093), *Lace^{k5305}* (#12176), *Lace^8* (#25150), *Schlank^{G0061}* (#11665), *Sply^{05091}* (#11393) *Lace*RNAi (#51475), Btl-GAL4 (#78328), Hemo-Gal4 (#78565), UAS-mCherry.nls (#38424), UAS-GFP-mCh-Atg8a (#37749), UAS-preproANF::GFP (#7001), UAS-Verm-RFP (#86530), UAS-Cht-Tom (#66512), *dASM*RNAi2 (#36760) Srp-Hemo-moe.mCherry (#78362), hs70FLP (#6416), neoFRT42D (#1802), neoFRT42D Ubi-mRFP.nls2R (#35496). The following stocks were obtained from the Vienna *Drosophila* Resource Centre (VDRC): sfGFP-CG3376 (#318772), *Schlank*RNAi (#v41114) and *dASM*RNAi1(#v12227). *dASM^k* was from Kyoto stock centre (#104944).

Cpes^{KO} and UAS-*Cpes* were gifts from Jairaj Acharya (NIH National Cancer Institute). The UAS-*hSmpd1* line was a gift from Hugo Bellen (Baylor College of Medicine).

Heterozygosity of *dASM* mutants was determined by the presence of CyO-GFP, which was visualised under the fluorescent dissecting microscope.

Embryo injections

Embryos were collected at 0–30 min of age, manually dechorionated and mounted in heptane glue under halocarbon oil (VWR). Desipramine, myriocin or water was backfilled into 3.5" Drummond capillary tubes and injected with a Picospritzer II microcellular injection unit at a consistent dose using an eyepiece graticule. Embryos were then allowed to develop at 25°C and viable embryos were scored for a tracheal phenotype.

Preparation of samples for targeted LC–MS/MS lipid analysis

The lipid-containing supernatant was extracted from sets of 300 stage 17 embryos using 300 ml MeOH, 600 ml chloroform. Extracts were centrifuged and 100 ml of 0.9% NaCl was added. The bottom phase of the biphasic extract was evaporated using a vacuum concentrator. Dried extracts were resuspended in MeOH, 80% containing the internal standards d3-Cer (Cayman chemicals, 24396). The samples were shaken on a rotational shaker at 1500 rpm for 15 min and sonicated for 15 min prior to centrifugation at 16 900 × g for five minutes. 70 μl supernatant was transferred to glass microvials.

Analysis of lipids by targeted LC–MS/MS

The samples were analysed using a triple quadrupole mass spectrometer (Waters Xevo TQ-S) equipped with an ESI source, coupled to a quaternary Waters Acquity liquid chromatographic separation system. Detection was performed in multiple reaction monitoring mode (MRM), where the transitions from precursor ions to class-specific fragment ions were monitored. Lipids were separated by normal phase chromatography on an ACQUITY UPLC BEH HILIC Column, 130 Å, 1.7 μm, 2.1 mm X 50 mm (Waters Corp Manchester UK) held at 55°C. Mobile phases were A: 95% ACN, 10 mM NH4Ac and B: 50% ACN, 10 mM NH4Ac. Starting conditions consisted of 100% A and increased to 100% B over 3.75 mins.

Data integration for lipidomic analysis

Data were acquired in MassLynx 4.2 and transformed into text files using the application MSConvert from the package ProteoWizard. Peak picking and integrations were performed

using an in-house application written in Python (available via the GitHub repository https://github.com/jchallqvist/mrmIntegrate), which rendered the area under the curve by the trapezoidal integration method. Each analyte was thereafter normalised to the d3-Cer internal standard.

Fluorescent microscopy

Live embryos were manually dechorionated, selected for genotype, staged on heptane glue on a microscope slide, immersed in halocarbon oil and placed beneath a coverslip. Tracheal sections were then immediately imaged using 1 μm z-slices with a 20× or 63× oil objective on a Zeiss 700 or Zeiss 880 confocal microscope.

Lysotracker and DHE staining was conducted as previously described (Evans *et al.* 2013). In brief, embryos were manually dechorionated, selected for genotype and transferred to Schneiders insect medium containing 50 nM Lysotracker™ Red DND-99 (Thermo Fisher) or DHE (Thermo Fisher). They were then incubated with shaking at 700 rpm for 30 min before mounting in PBS and immediately imaging at 63× on a Zeiss 700 confocal microscope.

Immunofluorescence

Stage 15/16 embryos were used for immunostaining as the cuticle remained partially penetrant for immunostain uptake at this stage of development. This was performed using a protocol adapted from [58]. In brief, embryos were dechorionated in 50% bleach (Acros Organics), washed in phosphate buffered saline-containing 0.5% tween-20 (PBS-T), and fixed nutating in scintillation vials in 4% paraformaldehyde in PBS-T for 20 min beneath a 1:1 heptane layer. Paraformaldehyde and heptane layers were then removed and replaced by a 1:1 heptane: methanol mix and shaken vigorously for 1 min. Devitellinised embryos were then washed 3× in methanol, followed by graded washes into PBS-T. Blocking was performed for 1 h in 5% horse serum (Gibco) in PBS-T. Embryos were then incubated for 2 days at 4°C in primary antibody, followed by 1 h of PBS-T washes and a further overnight incubation at 4°C in secondary antibody. Embryos were then mounted beneath a coverslip in VECTASHIELD mounting medium with DAPI and imaged on a Zeiss 700 confocal microscope. DSHB 2A12 GASP was used as the primary antibody (1:200) and the secondary antibody was A10001 goat-anti-mouse 488 (1:250).

Western blotting

3 repeats of 50 embryos were collected and flash frozen in liquid nitrogen. Embryos were manually homogenized with a micropestle in NuPage LDS sample buffer and 50 nM DTT, run on a NuPage 4%–12% Bis-Tris gel (Invitrogen) and transferred to a PVDF membrane [59]. Membranes were blocked in 5% milk powder in TBS-T (TBS with 0.1% Tween 20) for 1 h and probed by the following primary antibodies: Lamp1 (Abcam 30687, 1:2000), GABARAP (Abcam 109364, 1:2000), ASP175 (Cell Signalling 9661L, 1:2000) and Actin (Abcam 8224,1:10000). The following secondary antibodies were used: goat-anti-mouse-HRP (Abcam 6789, 1:10000) or goat-anti-rabbit-HRP (Abcam 67211:10000). Membranes were visualised with immobilon crescendo HRP reagent on an ImageQuant LAS4000. Bands were normalised to actin and quantified using ImageJ.

Mosaic generation

FRT42b sites were recombined onto the *dASM*^{k} chromosome and flies of the genotype hs70FLP. FRT42B ubi-RFP/FRT42B *dASM*^{k} were heat-shocked at 37°C for 1 h at the 3rd instar larval stage to induce

FLP/FRT-mediated cell-specific recombination. They were then aged to adulthood for 3 weeks. RFP negative cells denote *dASM*^{k} homozygous mosaic cells. Tissues were dissected in Schneider's media, and immediately imaged in 50 nM Lysotracker™ Green DND-26 (Thermo Fisher).

Supplementary data

Supplementary data is available at *HMG Journal* online.

References

1. Zampieri S, Filocamo M, Pianta A. *et al.* SMPD1 mutation update: database and comprehensive analysis of published and novel variants. *Hum Mutat* 2016;**37**:139–147.
2. Stenson PD, Ball EV, Mort M. *et al.* Human gene mutation database (HGMD): 2003 update. *Hum Mutat* 2003;**21**:577–581.
3. McGovern MM, Avetisyan R, Sanson BJ. *et al.* Disease manifestations and burden of illness in patients with acid sphingomyelinase deficiency (ASMD). *Orphanet J Rare Dis* 2017;**12**:41.
4. Gan-Or Z, Ozelius LJ, Bar-Shira A. *et al.* The p.L302P mutation in the lysosomal enzyme gene SMPD1 is a risk factor for Parkinson disease. *Neurology* 2013;**80**:1606–1610.
5. Gan-Or Z, Orr-Urtreger A, Alcalay RN. *et al.* The emerging role of SMPD1 mutations in Parkinson's disease: implications for future studies. *Parkinsonism Relat Disord* 2015;**21**:1294–1295.
6. Robak LA, Jansen IE, van Rooij J. *et al.* Excessive burden of lysosomal storage disorder gene variants in Parkinson's disease. *Brain* 2017;**140**:3191–3203.
7. den Jager WA. Sphingomyelin in Lewy inclusion bodies in Parkinson's disease. *Arch Neurol* 1969;**21**:615–619.
8. Spillantini MG, Crowther RA, Jakes R. *et al.* α-Synuclein in filamentous inclusions of Lewy bodies from Parkinson's disease and dementia with Lewy bodies. *Proc Natl Acad Sci USA* 1998;**95**:6469–6473.
9. Schissel SL, Schuchman EH, Williams KJ. *et al.* Zn2+−stimulated sphingomyelinase is secreted by many cell types and is a product of the acid sphingomyelinase gene. *J Biol Chem* 1996;**271**:18431–18436.
10. Kornhuber J, Rhein C, Muller CP. *et al.* Secretory sphingomyelinase in health and disease. *Biol Chem* 2015;**396**:707–736.
11. Galvan C, Camoletto PG, Cristofani F. *et al.* Anomalous surface distribution of glycosyl phosphatidyl inositol-anchored proteins in neurons lacking acid sphingomyelinase. *Mol Biol Cell* 2008;**19**:509–522.

12. Schuchman EH. Acid sphingomyelinase, cell membranes and human disease: lessons from Niemann-Pick disease. *FEBS Lett* 2010;**584**:1895–1900.

13. Diaz GA, Jones SA, Scarpa M. *et al*. One-year results of a clinical trial of olipudase alfa enzyme replacement therapy in pediatric patients with acid sphingomyelinase deficiency. *Genet Med* 2021;**23**:1543–1550.

14. Wasserstein MP, Lachmann R, Hollak C. *et al*. Continued improvement in disease manifestations of acid sphingomyelinase deficiency for adults with up to 2 years of olipudase alfa treatment: open-label extension of the ASCEND trial. *Orphanet J Rare Dis* 2023;**18**:378.

15. Lachmann RH, Diaz GA, Wasserstein MP. *et al*. Olipudase alfa enzyme replacement therapy for acid sphingomyelinase deficiency (ASMD): sustained improvements in clinical outcomes after 6.5 years of treatment in adults. *Orphanet J Rare Dis* 2023;**18**:94.

16. Lee PT, Zirin J, Kanca O. *et al*. A gene-specific T2A-GAL4 library for Drosophila. *elife* 2018;**7**:e35574.

17. Tomancak P, Berman BP, Beaton A. *et al*. Global analysis of patterns of gene expression during Drosophila embryogenesis. *Genome Biol* 2007;**8**:R145.

18. Sarov M, Barz C, Jambor H. *et al*. A genome-wide resource for the analysis of protein localisation in Drosophila. *elife* 2016;**5**:e12068.

19. Hayashi S, Kondo T. Development and function of the Drosophila tracheal system. *Genetics* 2018;**209**:367–380.

20. Levran O, Desnick RJ, Schuchman EH. Niemann-Pick disease: a frequent missense mutation in the acid sphingomyelinase gene of Ashkenazi Jewish type a and B patients. *Proc Natl Acad Sci USA* 1991;**88**:3748–3752.

21. Jones I, He X, Katouzian F. *et al*. Characterization of common SMPD1 mutations causing types A and B Niemann-Pick disease and generation of mutation-specific mouse models. *Mol Genet Metab* 2008;**95**:152–162.

22. Beitel GJ, Krasnow MA. Genetic control of epithelial tube size in the Drosophila tracheal system. *Development* 2000;**127**:3271–3282.

23. Tsarouhas V, Senti KA, Jayaram SA. *et al*. Sequential pulses of apical epithelial secretion and endocytosis drive airway maturation in Drosophila. *Dev Cell* 2007;**13**:214–225.

24. Gabande-Rodriguez E, Boya P, Labrador V. *et al*. High sphingomyelin levels induce lysosomal damage and autophagy dysfunction in Niemann Pick disease type A. *Cell Death Differ* 2014;**21**:864–875.

25. Kunduri G, Turner-Evans D, Konya Y. *et al*. Defective cortex glia plasma membrane structure underlies light-induced epilepsy in cpes mutants. *Proc Natl Acad Sci USA* 2018;**115**:E8919–E8928.

26. Pinto SN, Silva LC, Futerman AH. *et al*. Effect of ceramide structure on membrane biophysical properties: the role of acyl chain length and unsaturation. *Biochim Biophys Acta* 2011;**1808**:2753–2760.

27. Maula T, Al Sazzad MA, Slotte JP. Influence of hydroxylation, chain length, and chain unsaturation on bilayer properties of ceramides. *Biophys J* 2015;**109**:1639–1651.

28. Tsarouhas V, Liu D, Tsikala G. *et al*. A surfactant lipid layer of endosomal membranes facilitates airway gas filling in Drosophila. *Curr Biol* 2023;**33**:5132–5146.e5.

29. Morad SA, Cabot MC. Ceramide-orchestrated signalling in cancer cells. *Nat Rev Cancer* 2013;**13**:51–65.

30. Kurek K, Wiesiolek-Kurek P, Piotrowska DM. *et al*. Inhibition of ceramide de novo synthesis with myriocin affects lipid metabolism in the liver of rats with streptozotocin-induced type 1 diabetes. *Biomed Res Int* 2014;**2014**:980815.

31. Vos M, Klein C, Hicks AA. Role of ceramides and sphingolipids in Parkinson's disease. *J Mol Biol* 2023;**435**:168000.

32. Turpin-Nolan SM, Brüning JC. The role of ceramides in metabolic disorders: when size and localization matters. *Nat Rev Endocrinol* 2020;**16**:224–233.

33. Tringali C, Giussani P. Ceramide and Sphingosine-1-phosphate in neurodegenerative disorders and their potential involvement in therapy. *Int J Mol Sci* 2022;**23**:7806

34. Miyake Y, Kozutsumi Y, Nakamura S. *et al*. Serine Palmitoyltransferase is the primary target of a sphingosine-like immunosuppressant, Isp-1/Myriocin. *Biochem Biophys Res Commun* 1995;**211**:396–403.

35. Piper MD, Blanc E, Leitao-Goncalves R. *et al*. A holidic medium for Drosophila melanogaster. *Nat Methods* 2014;**11**:100–105.

36. Clayton RB. The utilization of sterols by insects. *J Lipid Res* 1964;**5**:3–19.

37. Carvalho M, Schwudke D, Sampaio JL. *et al*. Survival strategies of a sterol auxotroph. *Development* 2010;**137**:3675–3685.

38. Allen JA, Halverson-Tamboli RA, Rasenick MM. Lipid raft microdomains and neurotransmitter signalling. *Nat Rev Neurosci* 2007;**8**:128–140.

39. Musselman LP, Fink JL, Narzinski K. *et al*. A high-sugar diet produces obesity and insulin resistance in wild-type Drosophila. *Dis Model Mech* 2011;**4**:842–849.

40. Wasserstein M, Lachmann R, Hollak C. *et al*. A randomized, placebo-controlled clinical trial evaluating olipudase alfa enzyme replacement therapy for chronic acid sphingomyelinase deficiency (ASMD) in adults: one-year results. *Genet Med* 2022;**24**:1425–1436.

41. Rubins JB. Alveolar macrophages: wielding the double-edged sword of inflammation. *Am J Respir Crit Care Med* 2003;**167**:103–104.

42. Atilano ML, Hull A, Romila CA. *et al*. Autophagic dysfunction and gut microbiota dysbiosis cause chronic immune activation in a Drosophila model of Gaucher disease. *PLoS Genet* 2023;**19**:e1011063.

43. Hull A, Atilano ML, Gergi L. *et al*. Lysosomal storage, impaired autophagy and innate immunity in Gaucher and Parkinson's diseases: insights for drug discovery. *Philos Trans R Soc Lond Ser B Biol Sci* 2024;**379**:20220381.

44. Kinghorn KJ, Gronke S, Castillo-Quan JI. *et al*. A Drosophila model of Neuronopathic Gaucher disease demonstrates lysosomal-Autophagic defects and altered mTOR signalling and is functionally rescued by rapamycin. *J Neurosci* 2016;**36**:11654–11670.

45. Guillemot N, Troadec C, de Villemeur TB. *et al*. Lung disease in Niemann-Pick disease. *Pediatr Pulmonol* 2007;**42**:1207–1214.

46. McGovern MM, Aron A, Brodie SE. *et al*. Natural history of type A Niemann-Pick disease: possible endpoints for therapeutic trials. *Neurology* 2006;**66**:228–232.

47. McGovern MM, Wasserstein MP, Giugliani R. *et al*. A prospective, cross-sectional survey study of the natural history of Niemann-Pick disease type B. *Pediatrics* 2008;**122**:e341–e349.

48. Opoka L, Wyrostkiewicz D, Radwan-Rohrenschef P. *et al*. Combined emphysema and interstitial lung disease as a rare presentation of pulmonary involvement in a patient with chronic visceral acid sphingomyelinase deficiency (Niemann-Pick disease type B). *Am J Case Rep* 2020;**21**:e923394.

49. Sideris GA, Josephson M. Pulmonary alveolar proteinosis and Niemann Pick disease type B: an unexpected combination. *Respir Med Case Rep* 2016;**19**:37–39.

50. Poczobutt JM, Mikosz AM, Poirier C. *et al*. Altered macrophage function associated with crystalline lung inflammation in acid

sphingomyelinase deficiency. *Am J Respir Cell Mol Biol* 2021;**64**: 629–640.

51. Sezgin E, Levental I, Mayor S. *et al.* The mystery of membrane organization: composition, regulation and roles of lipid rafts. *Nat Rev Mol Cell Biol* 2017;**18**:361–374.

52. Holopainen JM, Angelova MI, Kinnunen PK. Vectorial budding of vesicles by asymmetrical enzymatic formation of ceramide in giant liposomes. *Biophys J* 2000;**78**:830–838.

53. Tam C, Idone V, Devlin C. *et al.* Exocytosis of acid sphingomyelinase by wounded cells promotes endocytosis and plasma membrane repair. *J Cell Biol* 2010;**189**:1027–1038.

54. Rietveld A, Neutz S, Simons K. *et al.* Association of sterol- and glycosylphosphatidylinositol-linked proteins with Drosophila raft lipid microdomains. *J Biol Chem* 1999;**274**:12049–12054.

55. Seppo A, Moreland M, Schweingruber H. *et al.* Zwitterionic and acidic glycosphingolipids of the Drosophila melanogaster embryo. *Eur J Biochem* 2000;**267**:3549–3558.

56. Guan XL, Cestra G, Shui G. *et al.* Biochemical membrane lipidomics during Drosophila development. *Dev Cell* 2013;**24**: 98–111.

57. Ile KE, Tripathy R, Goldfinger V. *et al.* Wunen, a Drosophila lipid phosphate phosphatase, is required for septate junction-mediated barrier function. *Development* 2012;**139**:2535–2546.

58. Sarkissian T, Timmons A, Arya R. *et al.* Detecting apoptosis in Drosophila tissues and cells. *Methods* 2014;**68**:89–96.

59. Madeira F, Madhusoodanan N, Lee J. *et al.* The EMBL-EBI job dispatcher sequence analysis tools framework in 2024. *Nucleic Acids Res* 2024;**52**:W521–W525.